Light-scattering study of modulated structure in a chiral smectic-*A* liquid crystal

Anlun Tang and S. Sprunt
Department of Physics, Kent State University, Kent, Ohio 44242
(Received 10 June 1997)

We use dynamic light scattering to investigate the fluctuation modes of a chiral smectic-*A* liquid crystal which exhibits a metastable one-dimensional modulation of the smectic layers parallel to the average layer plane. The modulation, which contains two components (a ''main'' and ''fine'' structure), breaks translational symmetry in the layer plane, and produces two new hydrodynamic fluctuation modes in addition to the director fluctuations. In a sufficiently large applied electric field, the modulation is destabilized: large amplitude fluctuations of the symmetry-restoring modes are observed. Both the frequency and dispersion of these modes change significantly from the zero field case. We present a phenomenological elastic theory, which quantitatively describes the measured dispersion of the mode frequencies and amplitudes, in both zero and high applied field. We also discuss how the transition from zero to high applied field might be understood in terms of recent theories of smectic phases with broken layer inversion symmetry, which predict a nontrivial renormalization of the elastic constants due to anharmonic fluctuations.
[S1063-651X(98)12003-2]

PACS number(s): 61.30.Eb, 78.35.+c

I. INTRODUCTION

Smectic liquid crystals composed of chiral molecules are of fundamental physical importance, because they exhibit a remarkable range of different phases and structural phase transitions which are uniquely associated with the presence of spontaneous polar order. They are also finding steadily increasing application in electro-optic technologies. In tilted chiral smectics, mirror symmetry is broken through the plane of the tilt [1], and a polarization $\vec{P}$ appears along the axis perpendicular to this plane—i.e., $\vec{P}$ is perpendicular to both the smectic layer normal and the molecular long axis (or director) $\vec{n}$. Under an applied electric field $\vec{E}$, $\vec{P}$—and consequently $\vec{n}$—can be rotated about the layer normal (Goldstone mode). In the smectic-*A* phase, however, both the tilt angle θ and $\vec{P}$ vanish, and mirror symmetry is broken only in the presence of an applied field $\vec{E}$ perpendicular to $\vec{n}$. The result is an *induced* polarization and a continuous variation of θ with E, or electroclinic effect. In this case, the motion of $\vec{n}$ corresponds to rotation about an axis perpendicular to the layer normal (soft mode).

In materials with large electroclinic effects, an additional broken symmetry has been recently observed [2], namely a uniaxial modulation of both the director and smectic layer orientation whose wave vector lies in the layer plane, along the tilt direction, and perpendicular to the induced polarization. Between crossed polarizers in the microscope, the modulation appears as a striking pattern of stripes, which run parallel to the average layer normal and alternate in contrast along the modulation direction. The amplitude of the modulation is a strong function of $\vec{E}$, but does not vanish when $\vec{E}\rightarrow 0$. This fact, together with careful optical and x-ray measurements [3,4] which indicate that the *average* tilt is zero for $E=0$, implies that the modulation does not arise strictly from shrinkage of the layer spacing in a tilted smectic, produced by minimizing the elastic energy at constant volume [5]. Alternative mechanisms, which have recently been proposed to explain modulated structure in ferroelectric liquid crystals, involve either a modulation of the local polarization stabilized by charged impurities [6] or a regular pattern of electrohydrodynamic flow of charged impurities [7], similar to Williams domains in nematic liquid crystals. Neither mechanism, however, has been confirmed in the chiral smectic-*A* phase.

In an earlier work [8], we addressed the key issue of the effects of the layer modulation on the fluctuation modes of the system. This problem is important since the dynamical consequences of the modulated structure are likely to impact the technical application of any high-polarization chiral smectic. Briefly, the layer modulation, which breaks continuous translational symmetry within the smectic layers, was shown to generate a new symmetry-restoring hydrodynamic mode, corresponding to undulations of the domain walls—or one-dimensional unit cell boundaries—of the modulation. The properties of this ''domain'' mode were explained by an elastic free energy based on a two-dimensional lattice with rectangular symmetry (broken translational symmetry along the modulation direction as well as in the direction of smectic layering). However, the mode was also found to be split into two components, which were attributed to distinct surface and bulk components of the layer modulation.

In the present paper, we expand on our previous results in two significant ways. First, we show that the splitting of the domain mode is in fact due to the presence of *two* modulations—a ''main'' and ''fine'' structure—which apparently coexist through the bulk of the sample. An extended theory, which includes both modulations, is successfully applied to a much more comprehensive set of dynamical data, and definitively establishes that the domain modes in zero field are associated with first order elastic restoring forces (i.e., broken translational symmetry). Second, we present new data taken in an applied dc electric field. The field destabilizes the modulated structure, producing very large fluctuations in the domain wall displacements. The correspond-

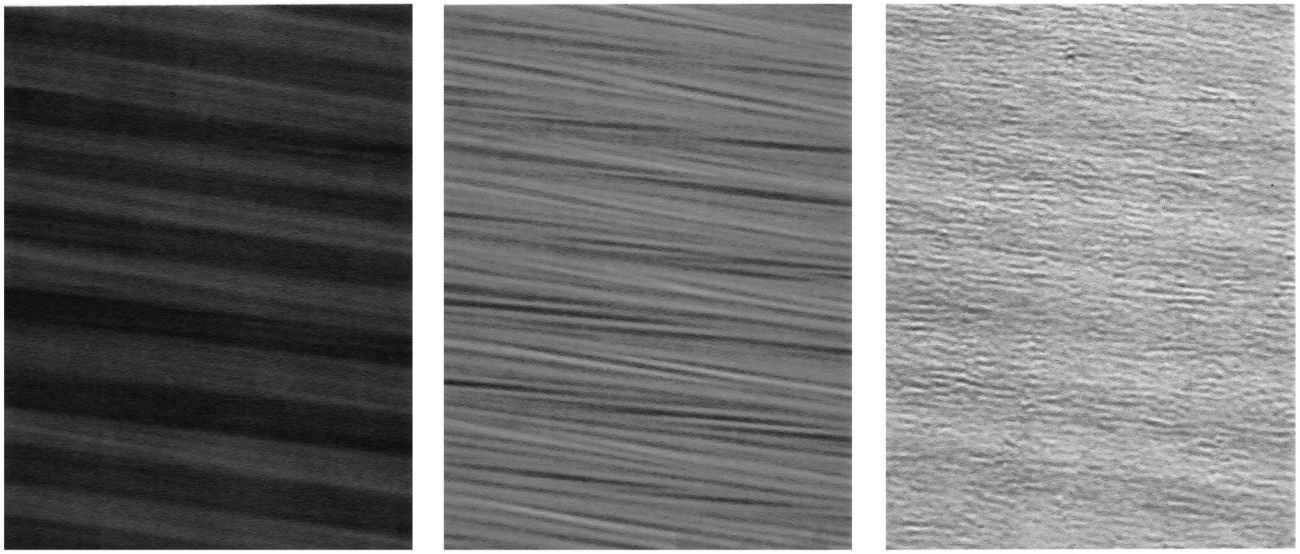

FIG. 1. Left: Optical micrograph showing the stripe texture characteristic of the layer-director modulation in the chiral smectic-*A* liquid crystal KN125 in zero field. The average director and smectic layer normal are parallel to the stripes. The main pattern has a periodicity comparable to the cell thickness (10 μm). A close examination reveals a fine structure within the main stripes. Middle: The fine structure modulation is clearly exposed in a weak applied field ($E=0.4$ V/μm). It has about one-fifth the period of and is roughly parallel to the main modulation. Right: In a large applied field ($E=12.5$ V/μm), the stripe structure is destabilized, and very large fluctuations of the domain walls of the modulation are observed. The stripes assume the appearance of rough interfaces.

ing dynamics differ significantly from the zero field case, but can still be described by our phenomenological model, with the domain mode dispersion now dominated by second order elastic constants and containing no contribution from first order elasticity. This result is discussed in light of recent theoretical predictions of strongly renormalized elastic constants due to anharmonic terms in the free energy of a chiral smectic liquid crystal.

II. EXPERIMENTAL DETAILS

The chemical structure of the liquid crystal studied (denoted KN125) is shown in Fig. 2. This material has a broad chiral smectic-*A* phase, $\sim 30\,^{\circ}$C to $78.3\,^{\circ}$C measured on heating. It can, however, be supercooled to ambient temperatures, where it is stable for several days to weeks. At 25 °C, the electroclinic coefficient is quite large, $(d\theta/dE)_{E=0}=4.5^{\circ}\,\mu$m/V, and the induced polarization is 70 nC/cm^2 at $E=15$ V/μm [9]. The sample was loaded in the isotropic phase into a 10 μm thick commercial cell, whose inside surfaces were coated with a transparent conducting layer (ITO) and a layer of polyimide, which is uniformly rubbed for homogeneous alignment of the liquid crystal. At the isotropic to smectic-*A* transition, the sample was exposed to a weak ac field (a 10 V square wave at 10 Hz) to assist in achieving uniform alignment. The uniaxial layer-director modulation is

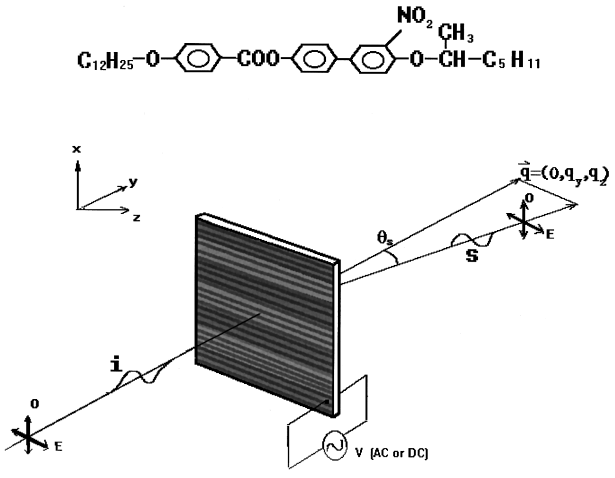

FIG. 2. The chemical structure of KN125 (above), and a schematic of our light scattering experiment. The polarizer and analyzer were arranged to probe either ordinary-extraordinary (OE) or EO scattering processes. The scattering vector $\vec{q}$ is perpendicular to the modulation direction $\hat{x}$, and varies as a function of scattering angle θ_s for normal incidence.

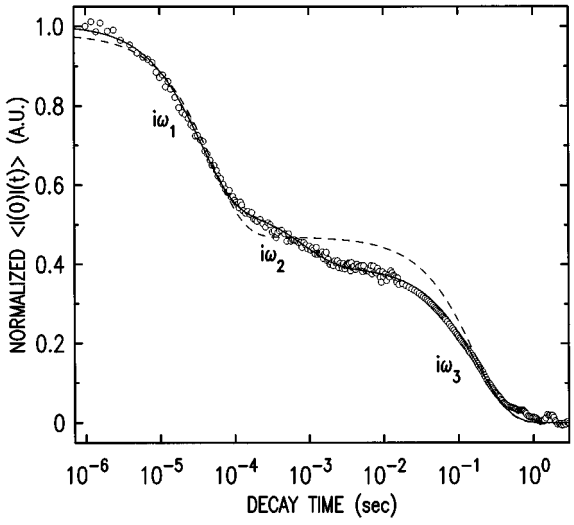

FIG. 3. A typical measurement of the zero-field time correlation function of the scattered intensity in the OE geometry. The solid (dashed) line represents a fit to three (two) overdamped modes.

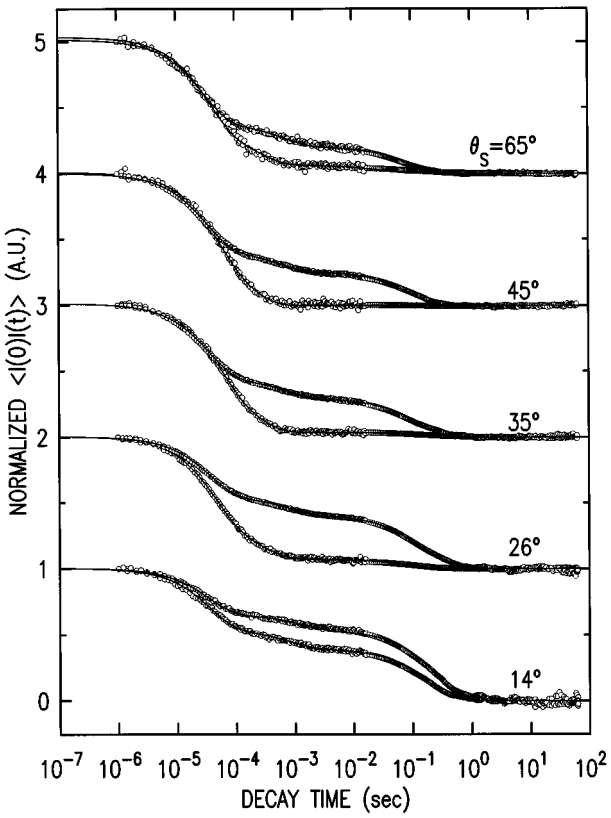

FIG. 4. Measured zero-field time correlation functions as a function of scattering angle θ_s for normal incidence. Upper (lower) curves are data for OE (EO) scattering processes. The solid lines are fits to three overdamped modes.

clearly observed in the polarizing microscope during cooling, and remains after the electric field is switched off. Figure 1 (top) is a microscopic picture of our sample of between crossed polarizers at 25 °C and $E=0$. The average director $\vec{n}_0$ is parallel to the stripe pattern within the $\pm 1°$ accuracy of our microscope measurement; thus, the stripes correspond to a spatial modulation of the director perpendicular to $\vec{n}_0$. The period d_0 is $\sim 10\,\mu$m (about equal to the cell thickness). Detailed x-ray measurements [3,10] have confirmed the optical modulation is accompanied by a modulation of the smectic layer orientation. A close examination of Fig. 1 (top) reveals a fine structure pattern *in addition* to the main stripes and roughly parallel to the main stripe direction. As shown in Fig. 1 (middle), this fine structure emerges clearly in a weak applied field ($E=0.4$ V/μm). The fine structure spacing is approximately 2 μm, and appears to be commensurate with the main stripe pattern.

A schematic of our light scattering experiment is shown in Fig. 2. Light from an argon-ion laser ($\lambda=488$ nm, incident power=10 mW, focused waist=100 μm) was normally incident on the sample. The position of the beam on the sample was adjusted to illuminate a region which gave sharp diffraction spots corresponding to the wave vector of the main layer-director modulation. Excellent alignment of $\vec{n}_0$ was indicated by a sharp minimum in the depolarized transmitted light, observed as $\vec{n}_0$ was rotated into and out of the scattering plane. The scattering angle θ_s was varied between 10° and 70°, and the sample was oriented so that the scattering vector $\vec{q}$ was maintained in a plane perpendicular to the modulation ($\hat{x}$ direction), giving $q_x=0$. Thus, only fluctuations along the average smectic layer normal $\hat{z}$, $q=q_z$, and in the smectic planes but perpendicular to the modulation direction, $q=q_y$, are detected. We measured the intensity-intensity time correlation function $\langle I(-\vec{q},0)I(\vec{q},t)\rangle$ of the depolarized scattered light as a function of θ_s for two combinations of polarizer and analyzer, referred to as OE (ordinary to extraordinary scattering process) and EO (extraordinary to ordinary). Correlation data were obtained in zero field and with a dc field of $E=15$ V/μm applied parallel to the smectic layers (y direction). We verified that no damage to the sample occurred by cycling the field, waiting one hour between cycles, and comparing both zero and high field correlation functions for different cycles. No essential differences were observed, although significant hysteresis (probably due to charge injection and removal) occurred.

III. RESULTS AND DISCUSSION: ZERO FIELD

Figure 3 shows a typical (normalized) correlation function obtained from our sample in zero field. One clearly observes two overdamped modes—a fast mode, frequency $\omega_1 \sim 10^4-10^5$ Hz, and a slow mode, $\omega_3 \sim 10$ Hz. We also see a weak additional mode (indicated by the arrow), with intermediate frequency ω_2. To demonstrate the presence of the intermediate mode, we compared fits of the data to two and three damped exponentials; the expression for the homodyne intensity correlation function is

$$\langle I(-\vec{q},0)I(\vec{q},t)\rangle = \left[\sum_{i=1}^{3} A_i \exp(-\omega_i(\vec{q})t)\right]^2 + B, \quad (3.1)$$

where A_i are the mode amplitudes, and B is the measured background. Clearly a reasonable fit to the data requires three modes. In Fig. 4 we show correlation data at several scattering angles (10°–68°) and at zero incident angle. In each case, the lower and upper plots correspond to OE and EO polarizer settings, respectively. We see that the OE data vary significantly with scattering angle, while the EO data are less insensitive to θ_s. The continuous solid lines are our three-mode fits. From these fits we obtain the dispersion relations of the modes for both the OE and EO cases. The results are plotted in Fig. 5. We find one dispersionless (nonhydrodynamic) mode (ω_1) and two dispersive (hydrodynamic) modes (ω_2 and ω_3). It is natural to expect that the slow hydrodynamic modes are associate with fluctuation of domain walls of the modulated structure, whereas the fast mode is associated with the so-called soft mode of the smectic-*A* phase, which corresponds to fluctuations of the liquid crystal director away from the layer normal.

We now discuss a phenomenological theory to explain these dynamics. Based on the results of previous x-ray studies [3,10], we assume that both the main and fine structure optical modulations of Fig. 1 mirror underlying modulations of the smectic layers. For simplicity, we assume that the modulations are sinusoidal in zero field. Figure 6 shows a schematic of the proposed structure. The equilibrium displacements of the smectic layers for the main and fine structure components are given by

$$u_{z0}^{(i)}(x) = u_0^{(i)} \sin(q_0^{(i)} x + \phi_0^{(i)}), \quad (3.2)$$

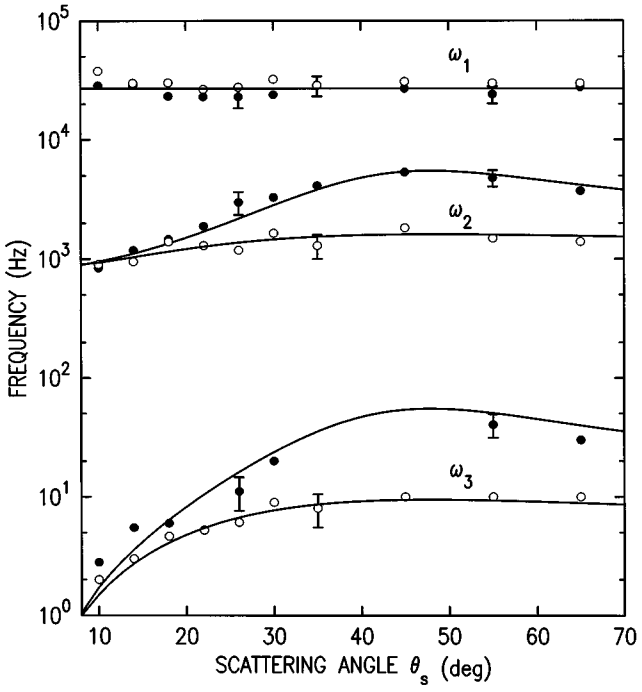

FIG. 5. Zero-field dispersion of the frequencies of the three overdamped modes corresponding to director (ω_1) and domain wall (ω_2 and ω_3) fluctuations (see text). Filled (open) circles correspond to the OE (EO) geometry, and solid lines are fits to Eqs. (3.12)–(3.14) of the text.

where $q_0^{(i)}$ and $\phi_0^{(i)}$ are the wave vectors and phases of the two modulations. The fluctuating part of the layer displacement is denoted u_z. The angles describing the smectic layer orientation are

$$\alpha^{(i)}(x)=\frac{\partial u_{z0}^{(i)}}{\partial x}=\alpha_0^{(i)}\cos(q_0^{(i)}x+\phi_0^{(i)}). \tag{3.3}$$

As determined by x-ray and optical measurements, the $\alpha_0^{(1)}$ for the main component is a few degrees in zero field and

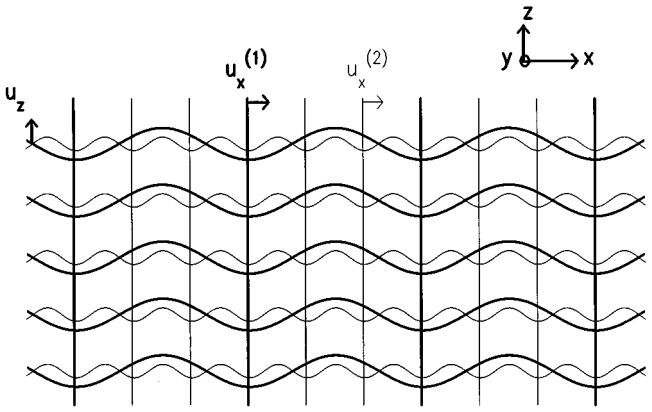

FIG. 6. Schematic of a model for the layer-modulated chiral smectic-*A* structure. The horizontal sine waves represent the two components of the layer modulation. Vertical lines indicate domain walls for the two components (here they are shown in phase). The displacement variables for the domain walls, as well as for the smectic layers, are indicated.

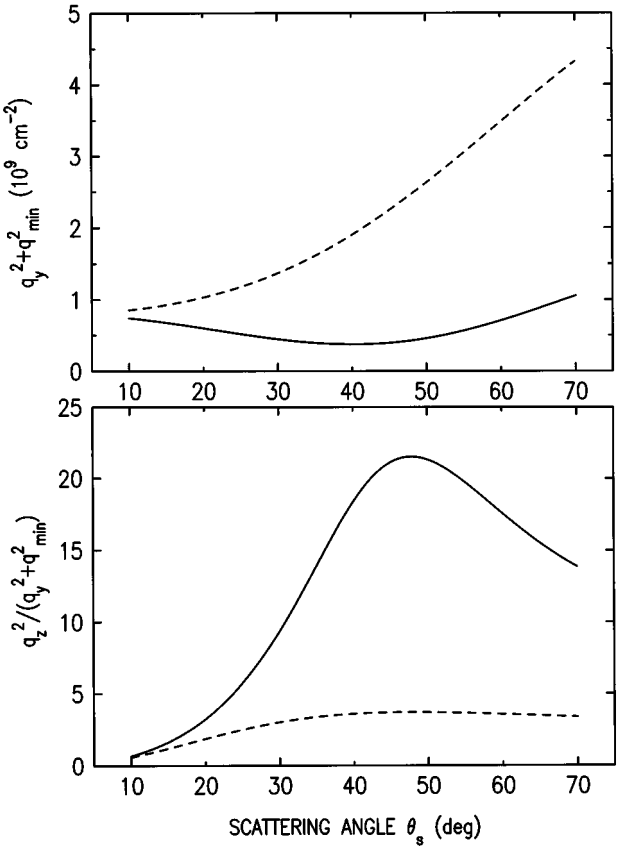

FIG. 7. Calculated curves showing the dependence on scattering angle of the two combinations of scattering vector components appearing in the dispersion relations for the fluctuation modes [Eqs. (3.12)–(3.14) of the text]. A low q_y cutoff, representing the finite cell thickness, has been imposed (see text).

$\alpha_0^{(2)}<\alpha_0^{(1)}$. The domain walls of the layer modulations are indicated by vertical lines; if we model these as ''super-smectic'' density waves, the associated ''layer'' displacements, denoted $u_x^{(i)}$, are continuous functions of x. The modulation breaks translational symmetry along the x direction, in addition to the usual broken symmetry of a smectic-*A* along the z axis. The symmetry in the x-z plane is rectangular (with a large anisotropy in the periodicities along x and z, $d_x/d_z\sim 10^3$), and is continuous along the y axis. We write the corresponding elastic free energy density as

$$\mathcal{F}=\frac{1}{2}\left[\sum_{i=1}^{2} C_1^{(i)}(\partial_x u_x^{(i)})^2+C_2(\partial_z u_z)^2\right]+\frac{1}{2}\sum_{i=1}^{2}[C_{12}^{(i)}(\partial_x u_z+\partial_z u_x^{(i)})^2+C_{12}'^{(i)}(\partial_x u_x^{(i)})(\partial_z u_z)]+\frac{1}{2}\left[\sum_{i=1}^{2} K_1^{(i)}(\partial_y^2 u_x^{(i)})^2+K_2(\partial_y^2 u_z)^2\right]+\frac{D}{2}(\vec{n}-\vec{l}^{\,s})^2+\frac{D'}{2}(\vec{l}^{\,(1)}-\vec{l}^{\,(2)})^2. \tag{3.4}$$

There are three types of terms in this expression: (i) terms describing deformations of the smectic layers and the domain walls of the modulated structure, which include first order elastic constants C for the broken symmetry directions x and z; (ii) terms containing second order elastic moduli K for fluctuations in the continuous symmetry direction y; and

(iii) coupling terms which favor parallel orientation of the director and smectic layer normal, $\vec{l}^S$, and of the domain wall normals for the two components of the layer-director modulation, $\vec{l}^{(1)}$ and $\vec{l}^{(2)}$. The normals are given by

$$\vec{l}^s=\frac{\vec{\nabla} f_s}{|\vec{\nabla} f_s|}, \tag{3.5}$$

where

$$f_s=z-nd_z-u_{z0}^{(1)}(x)-u_{z0}^{(2)}(x)-u_z(\vec{r})-\alpha^{(1)}(x)u_x^{(1)}(\vec{r}) -\alpha^{(2)}(x)u_x^{(2)}(\vec{r}) \tag{3.6}$$

and

$$\vec{l}^{(i)}=\frac{\vec{\nabla} f_i}{|\vec{\nabla} f_i|}, \tag{3.7}$$

where

$$f_i=x-nd_x^{(i)}-u_x^{(i)}(\vec{r}). \tag{3.8}$$

Equations (3.6) and (3.8) are correct to first order in the angles $\alpha^{(i)}$. The coupling between the director $\vec{n}$ and the domain wall fluctuations $u_x^{(i)}$, which is generated through Eqs. (3.4), (3.5), and the fourth term in the free energy density Eq. (3.3), is proportional to the $\alpha^{(i)}$. Since these are small quantities, the coupling terms may be treated as perturbations. The zero-order normal mode frequencies may then be calculated by diagonalizing the matrix form of $\mathcal{F}$ with the $\alpha^{(i)}$ set to zero. This calculation is further simplified if we assume the energy associated with compressing the smectic layers is effectively infinite (or $u_z=0$). Finally, taking $q_z=0$ for our experimental geometry and $q_z^2 \gg (q_0^{(i)})^2$ (typically $q_z \sim 6\ \mu\mathrm{m}^{-1}$, $q_0^{(1)} \sim 0.3\ \mu\mathrm{m}^{-1}$, and $q_0^{(2)} \sim 1.5\ \mu\mathrm{m}^{-1}$), we find

$$\mathcal{F}_0(\vec{q})=\frac{1}{2}\begin{array}{c} \\ n_x \\ n_y \\ q_y u_x^{(1)} \\ q_y u_x^{(2)} \end{array}\begin{array}{c} \begin{array}{cccc} n_x & n_y & q_y u_x^{(1)} & q_y u_x^{(2)} \end{array} \\ \begin{pmatrix} D & 0 & 0 & 0 \\ 0 & D & 0 & 0 \\ 0 & 0 & A^{(1)}(\vec{q})+D' & -D' \\ 0 & 0 & -D' & A^{(2)}(\vec{q})+D' \end{pmatrix} \end{array}, \tag{3.9}$$

where

$$A^{(1)}(\vec{q})=C_{12}^{(1)}q_z^2/q_y^2+K_1^{(1)}q_y^2, \tag{3.10}$$

$$A^{(2)}(\vec{q})=C_{12}^{(2)}q_z^2/q_y^2+K_1^{(2)}q_y^2. \tag{3.11}$$

The zero-order normal mode frequencies are

$$\omega_1=\frac{D}{\eta_1}, \tag{3.12}$$

$$\omega_2=\frac{1}{\eta_2}\,(C_{12}^{+}q_z^2/q_y^2+K_1^{+}q_y^2+D'), \tag{3.13}$$

$$\omega_3=\frac{1}{\eta_3}\,(C_{12}^{+}q_z^2/q_y^2+K_1^{+}q_y^2), \tag{3.14}$$

where the η_i are phenomenological damping coefficients, and

$$C_{12}^{+}\equiv\tfrac{1}{2}(C_{12}^{(1)}+C_{12}^{(2)}), \tag{3.15}$$

$$K_1^{+}\equiv\tfrac{1}{2}(K_1^{(1)}+K_1^{(2)}). \tag{3.16}$$

We also assume (and verify below) that

$$D'^2 \gg \tfrac{1}{4}(C_{12}^{(1)}-C_{12}^{(2)})^2=(C_{12}^{-})^2. \tag{3.17}$$

The first mode is the nonhydrodynamic mode associated with fluctuations of $\vec{n}$ away from the smectic layer normal, while the other two modes arise from in-phase and out-of-phase motion of the domain walls for the two components of the smectic layer modulation. The latter are q dependent, as anticipated from the data in Fig. 5. The key features of this dependence are illustrated in Fig. 7, which plots q_z^2/q_y^2 and q_y^2 for

$$q_z=k_0 \sin\theta_s \quad \text{(OE and EO)}, \tag{3.18}$$

$$q_y=k_0\left[\eta_{\|}\left(1-\frac{\sin^2\theta_s}{n_{\perp}^2}\right)^{1/2}-n_{\perp}\right] \quad \text{(OE)}, \tag{3.19}$$

$$q_y=k_0\left[n_{\|}-n_{\perp}\left(1-\frac{\sin^2\theta_s}{n_{\perp}^2}\right)^{1/2}\right] \quad \text{(EO)}, \tag{3.20}$$

where $k_0=2\pi/\lambda$. To account for the finite cell thickness t, we also imposed a low q_y cutoff, $q_{\min}\sim 2\pi/t$, by replacing q_y^2 in Eqs. (4.10) and (4.11) with $q_y^2+q_{\min}^2$. In the OE scattering geometry, we see that the q_z^2/q_y^2 and q_y^2 dependencies associated with the first and second order elastic constants are very different functions of θ_s. Moreover, q_z^2/q_y^2 changes between the OE and EO scattering geometries from a peaked to a smoothly increasing function of θ_s.

We now analyze the data for the dispersion of the three modes in Fig. 5 using Eqs. (3.12)–(3.14) and Eqs. (3.18)–(3.20). The refractive index $n_{\perp}$ and anisotropy Δn were fixed

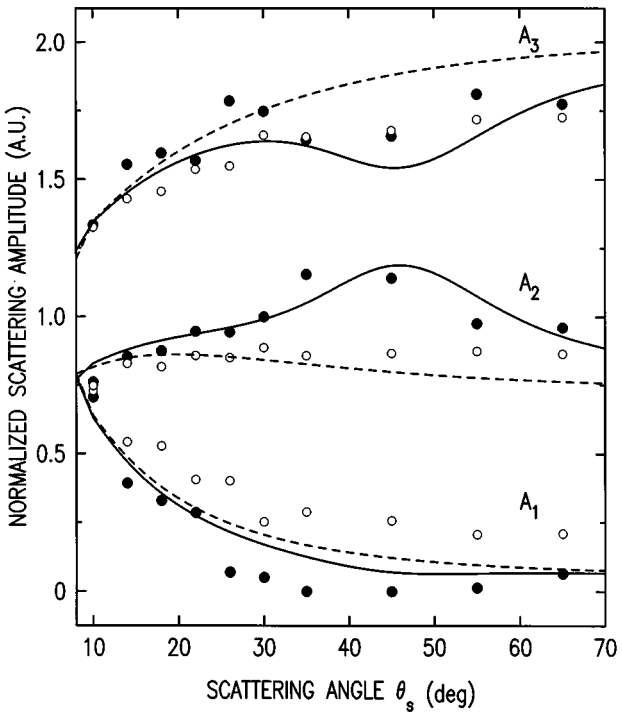

FIG. 8. Zero-field dispersion of the normalized amplitudes of the fluctuation modes for OE (closed symbols) and EO (open symbols) scattering. The solid (dashed) lines are fits to Eqs. (3.24)–(3.27) of the text for the EO (OE) data.

to typical values 1.51 and 0.16, respectively, during fitting. Of the six remaining parameters, D/η_1, C_{12}^{+}/η_2, C_{12}^{+}/η_3, D'/η_2, K_1^{+}/η_2, and K_1^{+}/η_3. The latter two were found to be unnecessary to describe the data. Indeed, Fig. 7 shows that the curvature of the OE data in Fig. 5 is consistent with a q_z^2/q_y^2 dependence and differs qualitatively from the q_y^2 behavior associated with the second order elasticities. Moreover, the shape of the data changes in the expected way between OE and EO scattering geometries. Thus, four parameters involving first order elastic constants only, plus the cutoff $q_{\min}$ were adjusted in the fits. Very good fits of all the data are obtained for $D/\eta_1 = 27\,000\ \mathrm{s}^{-1}$, $C_{12}^{+}/\eta_2 = 220\ \mathrm{s}^{-1}$, $C_{12}^{+}/\eta_3 = 2.6\ \mathrm{s}^{-1}$, and $D'/\eta_2 = 800\ \mathrm{s}^{-1}$. We also note that $D'^2 \sim 16 C_{12}^{+2} \gg C_{12}^{-2}$, which is consistent with the assumption in Eq. (3.17). The cutoff $q_{\min} = 1.88\times 10^6\ \mathrm{cm}^{-1}$ is about three times larger than $2\pi/t$. In fact, we expect an overestimate since we have assumed a simple step-function cutoff exactly at $2\pi/t$; the actual cutoff would be a smoothly varying function, presumably beginning at a shorter wavelength (higher q_y).

We have also analyzed the dependence of the normalized mode amplitudes $A_i/\Sigma_i A_i$, $i=1-3$ on θ_s for both OE and EO scattering geometries. The data are shown in Fig. 8; normalized amplitudes are plotted since we did not measure the absolute scattered intensity. To calculate the amplitudes, we first express the dielectric tensor fluctuations in terms of fluctuating components of the director for small $\alpha^{(i)}$, $\epsilon(\vec{q}) = \epsilon_a \cos\theta_s n_x(\vec{q})$ (OE scattering) and $\epsilon(\vec{q}) = \epsilon_a n_x(\vec{q})$ (EO scattering). (Fluctuations in n_y contribute to OE scattering only, but are weaker than n_x by a factor of order $\alpha^{(i)}$.) Next we must calculate the coupling of the domain modes to the director, since only the latter scatters light. This requires diagonalizing the free energy, Eq. (3.3), to first order in the coupling parameters $\alpha^{(i)}$ using a perturbative approach. We obtain

$$n_x(\vec{q}) = \psi_1(\vec{q}) - \frac{\sqrt{2}D}{(q_y^2+q_{\min}^2)^{1/2}}\left[\frac{q_-}{[\omega_1(\vec{q})\eta_1-\omega_2(\vec{q})\eta_2]}\,\psi_2(\vec{q}) - \frac{q_+}{[\omega_1(\vec{q})\eta_1-\omega_3(\vec{q})\eta_3]}\,\psi_3(\vec{q})\right], \tag{3.21}$$

where ψ_i are the zero order *normal* modes of the free energy, whose amplitudes can be calculated using the equipartition theorem

$$\langle \psi_i(-\vec{q})\psi_j(\vec{q})\rangle = \frac{k_B T}{\omega_i \eta_i}\,\delta_{ij} \tag{3.22}$$

and where

$$q_{\pm}^2 = (\alpha_0^{(1)} q_0^{(1)})^2 + (\alpha_0^{(2)} q_0^{(2)})^2 \pm 2\alpha_0^{(1)} q_0^{(1)} \alpha_0^{(2)} q_0^{(2)} \times \cos(\phi_0^{(1)} - \phi_0^{(2)}). \tag{3.23}$$

Combining these results, we obtain the scattering amplitudes for the three normal modes (for $q_x = 0$),

$$A_1(\vec{q}) = \frac{k_B T}{\eta_1 \omega_1(\vec{q})}, \tag{3.24}$$

$$A_2(\vec{q}) = \frac{k_B T}{\eta_2 \omega_2(\vec{q})}\,\frac{8q_-^2}{q_y^2+q_{\min}^2}\,\frac{1}{[1-\eta_3\omega_3(\vec{q})/\eta_1\omega_1(\vec{q})]^2}, \tag{3.25}$$

$$A_3(\vec{q}) = \frac{k_B T}{\eta_3 \omega_3(\vec{q})}\,\frac{8q_+^2}{q_y^2+q_{\min}^2}\,\frac{1}{[1-\eta_2\omega_2(\vec{q})/\eta_1\omega_1(\vec{q})]^2}, \tag{3.26}$$

for EO scattering, and

$$A_i(\vec{q}) \to \cos^2\theta_s A_i(\vec{q}) \tag{3.27}$$

for OE scattering. Figure 8 shows fits of the data for the normalized amplitudes $A_i/\Sigma_i A_i$, $i=1-3$, using Eqs. (3.24)–(3.27) and the fit parameters obtained from the previous analysis of the dispersion of the frequencies ω_i. Only four new parameters—the viscosity ratios η_2/η_1 and η_3/η_1 plus the dimensionless quantities $q_{\pm}/k_0$—are varied for all six data sets. (The cutoff $q_{\min}$, $n_\perp$, and Δn were also fixed to the values used in the fits to the frequencies). Clearly, the theoretical expressions give the correct qualitative behavior of the data. For the fit parameters, we find $\eta_2/\eta_1 = 3.3$ and $\eta_3/\eta_1 = 4.1$, and $q_+/k_0 = 0.017$, $q_-/k_0 = 0.002$. Referring back to Eq. (3.23), this implies $\phi_0^{(1)} - \phi_0^{(2)}$ lies between 90° and 180°; the simplest choice would be 180° (the two components of the modulation are out of phase with each other). Then taking $q_0^{(1)} = 2\pi/10 = 0.63\ \mu\mathrm{m}^{-1}$, we get $\alpha_0^{(1)} = 10°$, which is several times the zero-field limit extracted from x-ray scattering [3]. This discrepancy might indicate that the two components of the modulation are not pure sine waves

[as assumed in Eq. (3.2)]. In this case, the quantities $\alpha_0 q_0$ would be replaced by a series containing many harmonics of q_0. The sum of the coefficients α_0 in this series could be less than the single value calculated above. Moreover, the parameters $\alpha_\pm$ are rather sensitive to the cutoff $q_{\min}$ in Eqs. (3.25) and (3.26), and we have already noted that the simple form used for the cutoff may not be entirely accurate.

To summarize, our analysis of the normal mode frequencies and amplitudes, performed for two scattering processes with *distinct* $\vec{q}$ dependences and using only eight freely adjusted parameters for twelve data *sets*, demonstrates that the free energy density, Eq. (3.3), captures the essential features of the fluctuation spectrum of the layer-modulated chiral smectic-*A* liquid crystal. For the amplitudes, the theoretical description is less satisfactory, but is perhaps as good as could be expected from a first order calculation using a perturbative approach. Our results confirm the choice of the displacements $u_x^{(i)}$ as the appropriate phenomenological variables for the layer-director modulation. In zero field, the symmetry restoring modes corresponding to fluctuations of these variables can be adequately described by the first order elastic constants alone.

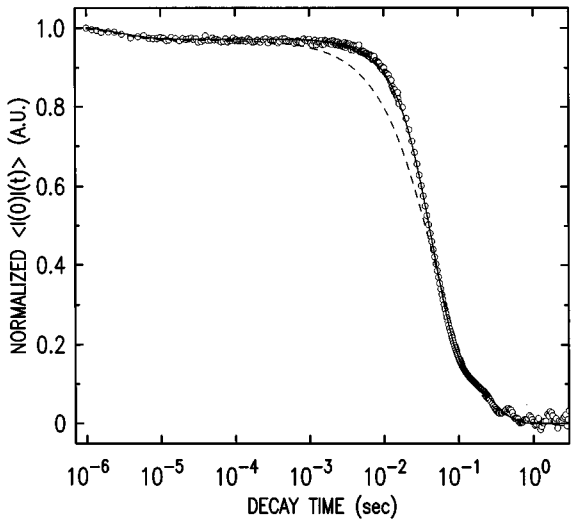

FIG. 9. A typical measurement of the high-field ($E = 12.5$ V/μm) time correlation function of the scattered intensity in the OE geometry. The solid (dashed) line represents a fit to three modes using stretched (pure) exponentials for the domain modes.

IV. RESULTS AND DISCUSSION: HIGH FIELD

Very different dynamics are observed in a high applied field. We applied a dc field of 15 V/μm; the dc field was used to avoid strong oscillating terms on the correlation function, which would obscure the overdamped dynamics. When the field is increased above a threshold value E_c ($E_c \sim 1.0$ V/μm), low-frequency macroscopic fluctuations of the domain walls associated with the fine structure can be observed; the fluctuation amplitudes become larger as the voltage is further increased until the fine structure is almost completely destabilized and significant amplitude fluctuations of the main structure are observed. This effect is shown in Fig. 1 (bottom), which is a microscope picture of our sample under a field of 12.5 V/μm. These large fluctuations dramatically alter the light scattering correlation function; Figs. 9 and 10 display data for $E = 15$ V/μm for the same scattering geometries used in zero field. The data differ significantly from the zero field case (Figs. 4 and 5). The nonhydrodynamic director mode is still present but is much weaker and faster. On the other hand, the hydrodynamic domain modes become slower and much stronger. Moreover, as Fig. 9 shows, we can no longer fit the correlation data with pure exponential decays as used in the zero-field case.

These results pose the question of whether we can analyze the *high-field* dynamics in terms of the phenomenological theory presented above. In particular, the large fluctuations in the domain wall displacements suggest that anharmonic terms in the $u_x^{(i)}$ variables should be incorporated in the analysis of the free energy. These terms would have two important effects for light scattering. First, the fluctuation amplitudes $\langle |u_x^{(i)}(\vec{q})|^2 \rangle$ would depend on renormalized harmonic elastic constants; for a certain class of smectic structure, this has been shown to be a very significant effect (see below) [11]. Second, anharmonic terms would lead to nonlinear dynamical equations, resulting in a coupling between fluctuations at different $\vec{q}$. Thus, the light scattered into the detector for a fixed setting $\vec{q}$ of our spectrometer will contain a spectrum of domain modes with wave vectors centered on $\vec{q}$. To account for this in our analysis of the correlation function, we assume that the resolution function for scattering from these modes is broadened from essentially a δ function $R(\vec{q}') = \delta(\vec{q} - \vec{q}')$ to a function of the form $R(\vec{q}')$

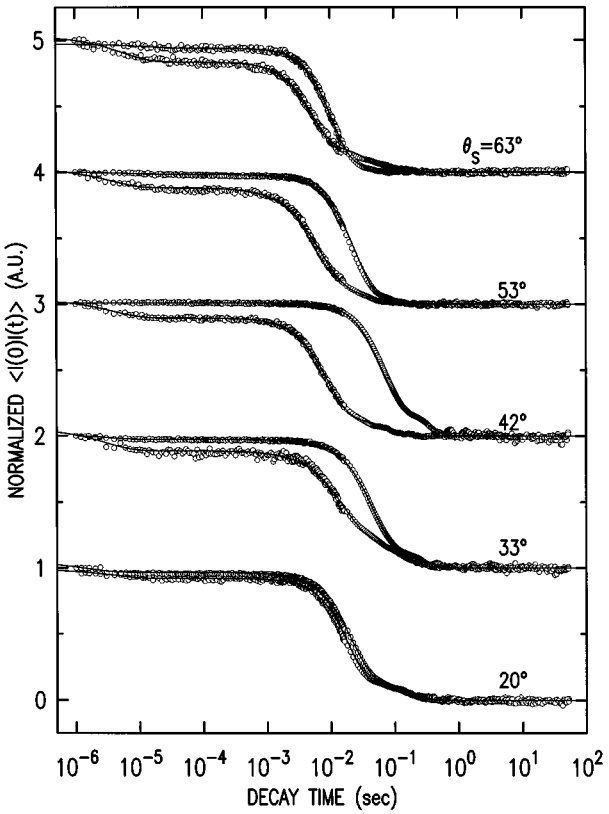

FIG. 10. Measured high-field time correlation functions as a function of scattering angle θ_s for normal incidence. Upper (lower) curves are data for OE (EO) scattering processes. The solid lines are fits to three overdamped modes using Eq. (4.2) of the text.

$\sim\exp(-w_i|q_i-q_i'|^n)$, where n is non-negative and we assume the broadening can be anisotropic in $\vec{q}$, since the allowed anharmonic terms are [11]. If R is normalized to unity, for $n\to\infty$, we recover $R(\vec{q}\,')\sim\delta(\vec{q}-\vec{q}\,')$.

Including the director mode, which to first order is decoupled from the domain wall displacements, the measured correlation function is

$$\langle I(-\vec{q},0)I(\vec{q},t)\rangle=\left[\sum_{i=1}^{2}\int d\vec{q}\,'R(\vec{q}\,')A_i(\vec{q}\,')\exp[-\omega_i(\vec{q}\,')t]+A_3(\vec{q})\exp(-\omega_3(\vec{q})t)\right]^2+B. \tag{4.1}$$

If we now approximate the frequencies by their lowest order values (linear dynamics), the q-dependent part of the frequencies is $\omega_i(\vec{q})=\Gamma_i q^2$. (This form applies if *second* order elasticity dominates the free energy, which is consistent with our results from analysis of the high field data discussed below.) Then the first terms in Eq. (4.1) are proportional to $\int d\vec{q}\,'\exp(-w_j|q_j-q_j'|^n)A_i(\vec{q}\,')\exp[-i\Gamma_i q'^2 t]$, which at long times corresponds to a stretched exponential time dependence [12],

$$\langle I(-\vec{q},0)I(\vec{q},t)\rangle\simeq\left[\sum_{i=1}^{2}A_i'(\vec{q})\exp[-(\omega_i(\vec{q})t)^x]+A_3(\vec{q})\exp(-\omega_3(\vec{q})t)\right]^2+B, \tag{4.2}$$

where the exponent $x\simeq n/(n-2)$ [12], and the A_i' may differ from A_i depending on the details of $R(\vec{q})$. Clearly this result is sensible only for $n>2$, or $x>1$. This function has been used extensively to model overdamped dynamics where a distribution of fluctuations characterized by different values of some property (here the wave vector $\vec{q}$) contributes. It has the additional virtue of adding only one more parameter (the exponent x) to fits of the correlator data. As shown in Figs. 9 and 10, the function does indeed describe the data well (with $x\simeq1.5$ in all the fits), in contrast to a pure exponential ($x=1$).

The mode frequencies obtained from these fits are presented in Fig. 11. We notice that the director mode is an order of magnitude faster at $E=15$ V/μm than in zero field; the nonhydrodynamic gap D/η_1 now has a value of 240 000 s^{-1} (versus 27 000 s^{-1}). In addition, the dispersion of the domain modes changes from a convex to a concave shape—or from a functional form given by q_z^2/q_y^2 (associated with the first order elastic constant C_{12}^+, see Fig. 7) to the form q_y^2 (associated with the second order elasticity K_1^+). The fits to the data using Eqs. (3.12)–(3.14) confirm this crossover. We obtain $K_1^+/\eta_2=1.1\times10^{-8}$ s^{-1} cm^2 and $K_1^+/\eta_3=2.2\times10^{-10}$ s^{-1} cm^2 with $C_{12}^+=0$. The gap parameter D'/η_3 has the same value as in zero field, and the parameters $n_\perp$, Δn, and $q_{\min}$ were fixed to the zero-field values.

We now consider a possible explanation for these results based on anharmonic fluctuations of the domain wall displacements. According to a recent theoretical analysis [11], anharmonic terms arising specifically in smectics, which lack inversion symmetry through the layer plane, can produce a nontrivial renormalization of the elastic constants. Specifically, the displacement fluctuations diverge as *power laws* of the system size L, and the elastic constants C and K undergo a softening proportional to inverse powers of L. The first order elasticities, however, soften more rapidly, $C\sim K^3\sim1/L^{3/4}$. Thus, under an external stress (e.g., applied field), it is possible to observe very large displacement fluctuations described purely by second order elasticity without destruction of the smectic layers. If we consider the domain walls of the modulated structure to represent layers of a ''supersmectic'' structure, this scenario is similar to what is observed in Fig. 1 (bottom) and in the crossover of the dynamics. It remains, however, to verify that the domain walls lack inversion symmetry. This we cannot do without a detailed explanation for the origin of the modulated structure. At present we can only speculate that if charged impurities play an important role, a domain wall could represent the interface between a region dominated by the influence of positive ions and one dominated by negative ions—in this case, the domain walls (or smectic ''layers'') would lack inversion symmetry. On the other hand, if the modulation is purely a consequence of minimizing elastic energy, the domain walls have no special microscopic meaning, and there is no basis for breaking inversion symmetry.

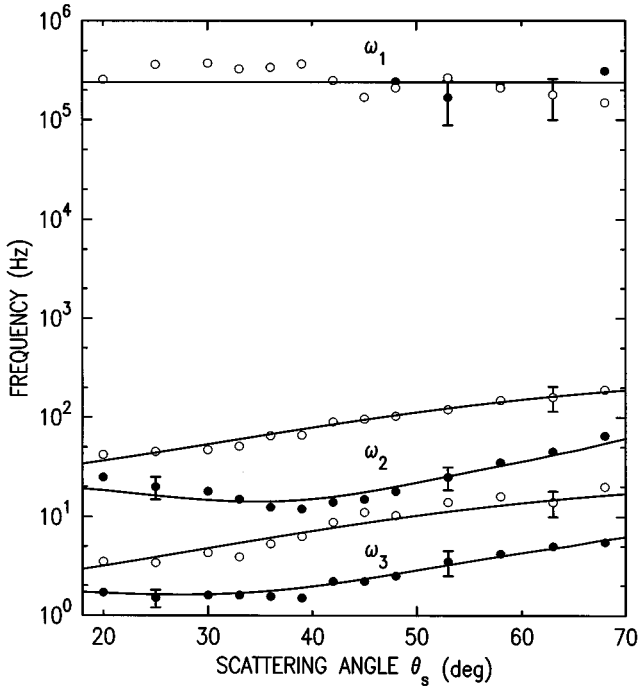

FIG. 11. High-field dispersion of the frequencies of the three overdamped modes corresponding to director (ω_1) and domain wall (ω_2 and ω_3) fluctuations. Filled (open) circles correspond to the OE (EO) geometry, and the solid lines are fits to Eqs. (3.12)–(3.14) of the text.

The sharp change in the frequency and relative amplitude of the high frequency director mode can be understood by considering the additional terms $-\vec{P}\cdot\vec{E}+\Delta\epsilon(\vec{E}\cdot\vec{n})^2/2=-P(\vec{n}\times\vec{l}^S)\cdot\vec{E}+\Delta\epsilon(\vec{E}\cdot\vec{n})^2/2$, which are present in the free

energy density for nonzero $\vec{E}$. (Here, $\vec{P}$ is the polarization due specifically to field-induced chiral symmetry breaking.) To second order in the director fluctuations n_x and n_y, this gives $PE \sin\theta n_x^2/2 + \Delta\epsilon E^2 n_y^2/2$. As remarked in Sec. III, we may neglect the second term, since the scattering from fluctuations in n_y is expected to be much weaker than n_x. Then the frequency ω_1 gets an additional contribution $PE \sin\theta/2\eta_1$, which will dominate at high field. We can estimate this contribution using the measured $P = 70\ \mathrm{nC/cm^2}$ and $\theta = 15°$ at $E = 15\ \mathrm{V}/\mu\mathrm{m}$ and taking $\eta_1 = 4$ cP (a typical value). We then obtain $\omega_1 = 200\,000\ \mathrm{s}^{-1}$, in good agreement with the measured value in Fig. 11.

V. CONCLUSION

In this paper, we have shown that chiral smectic-*A* liquid crystals, in which the orientation of normally flat layers is modulated in one dimension, exhibit new, symmetry-restoring fluctuation modes. These modes correspond to motion of the unit cell boundaries (or ''domain walls'') of the modulation; both their frequency and amplitude dispersion can be reasonably explained at the phenomenological level by an elastic free energy density, which includes two observed components of the modulation. In the absence of applied fields, the domain modes are controlled by first order elasticity, characteristic of a solid (broken translational symmetry). However, a sufficiently high electric field destabilizes the modulated structure, and results in a substantial softening of the first order elasticity. The domain modes are now dominated by second order elasticity, characteristic of a fluid. A significant softening of first order elasticity has in fact been predicted in systems with smectic structure under external stress, if the smectic layers lack inversion symmetry. If this idea is applicable to the domain walls of the layer-director modulation (visualized as ''super-smectic'' layers), it suggests that the latter should have some microscopic structure which breaks inversion symmetry. A likely mechanism—and one which could significantly alter the dynamics in an applied electric field—is a nonuniform distribution of charged impurities [6,7], which are known to give rise to ''ion'' modes in ferroelectric liquid crystals [13]. Light scattering experiments in an ac field, to look for characteristic cutoff frequencies in the response of the domain modes and thereby probe possible electrohydrodynamic effects in the modulated chiral smectic-*A* phase, are currently underway.

ACKNOWLEDGMENTS

This research was supported by the NSF's Advanced Liquid Crystalline Optical Materials Science and Technology Center, under Grant No. DMR-8920147. We have benefitted from useful discussions with B. Ratna, J. V. Selinger, and R. Shashidhar.

[1] R. B. Meyer, L. Liebert, L. Strzelecki, and P. Keller, J. Phys. (France) Lett. **30**, 69 (1975).
[2] S. Garoff and R. B. Meyer, Phys. Rev. Lett. **38**, 848 (1977); Phys. Rev. A **19**, 338 (1979).
[3] G. P. Crawford, R. E. Geer, J. Naciri, R. Shashidhar, and B. R. Ratna, Appl. Phys. Lett. **65**, 2937 (1994).
[4] K. Skarp, G. Andersson, T. Hirai, A. Yoshizawa, K. Hiraoka, H. Takezoe, and A. Fukuda, Jpn. J. Appl. Phys., Part 1 **31**, 1409 (1992); R. Shao, P. C. Willis, and N. A. Clark, Ferroelectrics **121**, 127 (1991).
[5] J. Pavel and M. Glogorova, Liq. Cryst. **9**, 87 (1991).
[6] S. A. Pikin, L. A. Beresnev, S. Hiller, M. Pfeiffer, and W. Haase, Mol. Mater. **3**, 1 (1993).
[7] A. B. Davey and W. A. Crossland, Mol. Cryst. Liq. Cryst. Sci. Technol., Sect. A **263**, 325 (1995).
[8] S. Sprunt, J. V. Selinger, G. P. Crawford, B. R. Ratna, and R. Shashidhar, Phys. Rev. Lett. **74**, 4671 (1995).
[9] G. P. Crawford, J. Naciri, R. Shashidhar, P. Keller, and B. R. Ratna, Mol. Cryst. Liq. Cryst. Sci. Technol., Sect. A **263**, 223 (1995).
[10] A. Rappaport, P. A. Williams, B. N. Thomas, N. A. Clark, M. B. Ros, and D. M. Walba, Appl. Phys. Lett. **67**, 362 (1995).
[11] L. Golubovic and Z. Wang, Phys. Rev. Lett. **69**, 2535 (1992).
[12] V. Degiorgio, R. Piazza, F. Mantegazza, and T. Bellini, J. Phys.: Condens. Matter **2**, SA69 (1990); M. H. Cohen and G. S. Grest, Phys. Rev. B **24**, 4091 (1981).
[13] M. H. Lu and C. Rosenblatt, Phys. Rev. E **48**, R2370 (1993).